

# Reduced exercise capacity occurs before intrinsic skeletal muscle dysfunction in experimental rat models of pulmonary hypertension

Peng Zhang<sup>1,2</sup> | Denielli Da Silva Goncalves Bos<sup>1,2,3</sup> | Alexander Vang<sup>1</sup> |  
Julia Feord<sup>1</sup> | Danielle J. McCullough<sup>4</sup> | Alexandra Zimmer<sup>1,2</sup> |  
Natalie D'Silva<sup>1,2</sup> | Richard T. Clements<sup>1,5</sup> | Gaurav Choudhary<sup>1,2</sup> 

<sup>1</sup>Vascular Research Laboratory, Providence VA Medical Center, Providence, Rhode Island, USA

<sup>2</sup>Division of Cardiology, Department of Medicine, Alpert Medical School of Brown University, Providence, Rhode Island, USA

<sup>3</sup>Pulmonary Division, Heart Institute, University of São Paulo Medical School, São Paulo, Brazil

<sup>4</sup>Medical Education, Edward Via College of Osteopathic Medicine, Auburn, Alabama, USA

<sup>5</sup>Biomedical and Pharmaceutical Sciences, University of Rhode Island, Kingston, Rhode Island, USA

## Correspondence

Gaurav Choudhary, Vascular Research Laboratory, Providence VA Medical Center, 830 Chalkstone Ave., Providence, RI 02908, USA.

Email: [gaurav\\_choudhary@brown.edu](mailto:gaurav_choudhary@brown.edu)

## Funding information

U.S. Department of Veterans Affairs, Grant/Award Number: I01CX001892; National Heart, Lung, and Blood Institute, Grant/Award Numbers: R01HL135236, R01HL148727; National Institute of General Medical Sciences, Grant/Award Number: 5P20GM103652; National Institute of General Medical Science of the National Institutes of Health, Grant/Award Number: P20GM103652; VA Merit Review, Grant/Award Number: I01CX001892; NHLBI, Grant/Award Numbers: R01HL148727, R01HL135236; NIGMS/NIH, Grant/Award Number: 5P20GM103652

## Abstract

Reduced exercise capacity in pulmonary hypertension (PH) significantly impacts quality of life. However, the cause of reduced exercise capacity in PH remains unclear. The objective of this study was to investigate whether intrinsic skeletal muscle changes are causative in reduced exercise capacity in PH using preclinical PH rat models with different PH severity. PH was induced in adult Sprague–Dawley (SD) or Fischer (CDF) rats with one dose of SU5416 (20 mg/kg) injection, followed by 3 weeks of hypoxia and additional 0–4 weeks of normoxia exposure. Controls rats were injected with vehicle and housed in normoxia. Echocardiography was performed to assess cardiac function. Exercise capacity was assessed by VO<sub>2</sub> max. Skeletal muscle structural changes (atrophy, fiber type switching, and capillary density), mitochondrial function, isometric force, and fatigue profile were assessed. In SD rats, right ventricular systolic dysfunction is associated with reduced exercise capacity in PH rats at 7-week timepoint in comparison to control rats, while no changes were observed in skeletal muscle structure, mitochondrial function, isometric force, or fatigue profile. CDF rats at 4-week timepoint developed a more severe PH and, in addition to right ventricular dysfunction, the reduced exercise capacity in these rats is associated with skeletal muscle atrophy; however, mitochondrial function, isometric force, and fatigue profile in skeletal muscle remain unchanged. Our data suggest that cardiopulmonary

This is an open access article under the terms of the [Creative Commons Attribution-NonCommercial](https://creativecommons.org/licenses/by-nc/4.0/) License, which permits use, distribution and reproduction in any medium, provided the original work is properly cited and is not used for commercial purposes.

© 2024 The Authors. *Pulmonary Circulation* published by John Wiley & Sons Ltd on behalf of Pulmonary Vascular Research Institute. This article has been contributed to by U.S. Government employees and their work is in the public domain in the USA.

impairments in PH are the primary cause of reduced exercise capacity, which occurs before intrinsic skeletal muscle dysfunction.

**KEYWORDS**

mitochondrial function, peripheral muscle function in lung disease, pulmonary hypertension

Pulmonary hypertension (PH) is defined with mean pulmonary arterial pressure greater than 20 mmHg at rest.<sup>1</sup> Despite contemporary therapy, PH patients experience symptoms that significantly impact their quality of life.<sup>2,3</sup> Among them, exercise intolerance is one of the predominant symptoms in PH and exercise capacity has been considered as an important indicator for prognosis.<sup>4–6</sup> However, the mechanisms underlying impaired exercise capacity in PH remain unclear and are important in designing novel interventions.

In addition to the structural alterations in pulmonary circulation in PH, there is development of right ventricular (RV) dysfunction and failure consequent to high RV afterload, which is associated with high morbidity and mortality.<sup>7,8</sup> In the traditional view, reduced exercise capacity in PH is mainly due to central cardiopulmonary impairments and systemic circulation dysfunction as primary factors. Recently, some evidence suggested that intrinsic dysfunction of peripheral skeletal muscle morphology and function may also be involved in the exercise limitation observed in PH and impaired exercise capacity.<sup>9,10</sup> This premise is based on observed changes in skeletal muscle including muscle atrophy, fiber type switching, less capillary density, reduced speed and strength of contraction, reduced systemic oxygen extraction, impaired mitochondrial function with reduced oxidative phosphorylation, and/or alterations in signaling cascades in PH patients and preclinical animal models.<sup>9–14</sup> In contrast, other studies have reported no intrinsic functional changes in peripheral skeletal muscle in PH.<sup>15,16</sup> This discrepancy highlights a potential dichotomy of exercise intolerance in PH in a model and disease severity-specific manner. It also raises a question on whether intrinsic skeletal muscle dysfunction is causative and detrimental to exercise intolerance in PH.

In this study, we performed a comprehensive investigation to evaluate skeletal muscle intrinsic changes and exercise capacity using preclinical PH rat models showing different PH severity. We chose soleus muscles in this study, because soleus muscles predominantly contain slow oxidative (Type I) muscle fibers in mature rats<sup>17</sup> and are one of the major skeletal muscles used by rats during exercise. Select assessments were also

done on the extensor digitorum longus (EDL) muscles (predominantly containing Type II muscle fibers) as another muscle type in severe PH animals. PH was induced in adult Sprague–Dawley (SD) or Fischer (CDF) rats with one dose of SU5416 (20 mg/kg) injection, followed by 3 weeks of hypoxia and additional 0–4 weeks of normoxia exposure. Strain, age, and gender-matched rats injected with vehicle and housed in normoxia for the duration of the experiments were used as controls. We assessed RV dysfunction using echocardiography and evaluated exercise capacity by measuring  $\text{VO}_2$  max. Three weeks and 7-week timepoints were used for SD rats and 4-week timepoint were used for CDF rats, representing a gradual increase of PH severity as the PH CDF rats show more severe PH than the PH SD rats and start to die at the 5-week timepoint. We investigated (1) structural changes including muscle atrophy, fiber type switching, and capillary density, (2) mitochondrial function assessed by high-resolution respirometry using permeabilized muscle fibers, (3) isometric force and fatigue profile assessments using isolated soleus muscle *ex vivo*, and (4) alterations of signaling cascades that regulate metabolism and mitochondrial biogenesis. Our study demonstrated that reduced exercise capacity in PH occurs in the absence of intrinsic functional changes in skeletal muscle, suggesting that alterations in skeletal muscle are not causative to exercise intolerance in PH. Therefore, our results suggest that improving central cardiopulmonary impairments at the early stage of PH may be critical in preventing or delaying the occurrence of exercise limitation in settings of PH.

## METHODS

### Rat models of PH

Male and female adult Sprague–Dawley rats (SD; 176–200 g, strain: 001) and Fischer (CDF; 150–175 g, strain: 002) were purchased from Charles River and randomly assigned to either control or PH groups. PH (SuHx model) was induced as previously described<sup>18,19</sup> by a single subcutaneous injection of a vascular endothelial growth factor receptor inhibitor (SU5416,

20 mg/kg body mass; APExBIO) that was dissolved in a diluent containing 0.5% carboxymethylcellulose, 0.9% NaCl, 0.4% Polysorbate 80, and 0.9% benzyl alcohol, followed by 3 weeks of normobaric hypoxia exposure (10% FiO<sub>2</sub>; Biospherix Ltd.) and subsequently housing them at normoxic conditions for additional 0–4 weeks. The control group (strain, age, and gender-matched rats) received a diluent injection and was housed in normoxic condition for the respective duration of the PH groups. At the end of Weeks 3 and 7 for SD rats (Figure 1a) or 4 weeks for CDF rats (Figure 5a), the animals were used for in vivo functional assessments, followed by tissue collection for ex vivo studies and biochemical analysis. Fulton index was calculated by RV weight divided by LV and septum weight (LV + S).

### Invasive hemodynamic measurements

Using an open-chest technique and a high-fidelity Millar 2.0 F catheter (SPR-869), RV systolic pressure (RVSP) was measured under isoflurane anesthesia (1.5%–2%). Steady-

state recordings were acquired for at least 30 s with a sampling rate of 2 kHz using PowerLab Data Acquisition system together with LabChart 8 software (ADInstruments).

### Echocardiographic measurement

Animals were anesthetized with continuous isoflurane inhalation (1.5%–2%) and transthoracic echocardiography was performed using Vevo2100 with S250 transducer (VisualSonics) as previously described.<sup>18,20</sup> Two-dimensional, Doppler and M-mode recordings were obtained to measure RV wall thickness and volumes. Left ventricular outflow tract (LOVT) diameter was measured in parasternal long axis view and used to calculate LVOT area which was then multiplied to velocity time integral of the Doppler flow across the LVOT in using apical views to calculate stroke volume. Cardiac output (CO) was calculated by stroke volume × heart rate. The pulsed-wave Doppler recording at the RV overflow tract was used to measure pulmonary acceleration time (PAT). Tricuspid annular plane systolic excursion (TAPSE) was

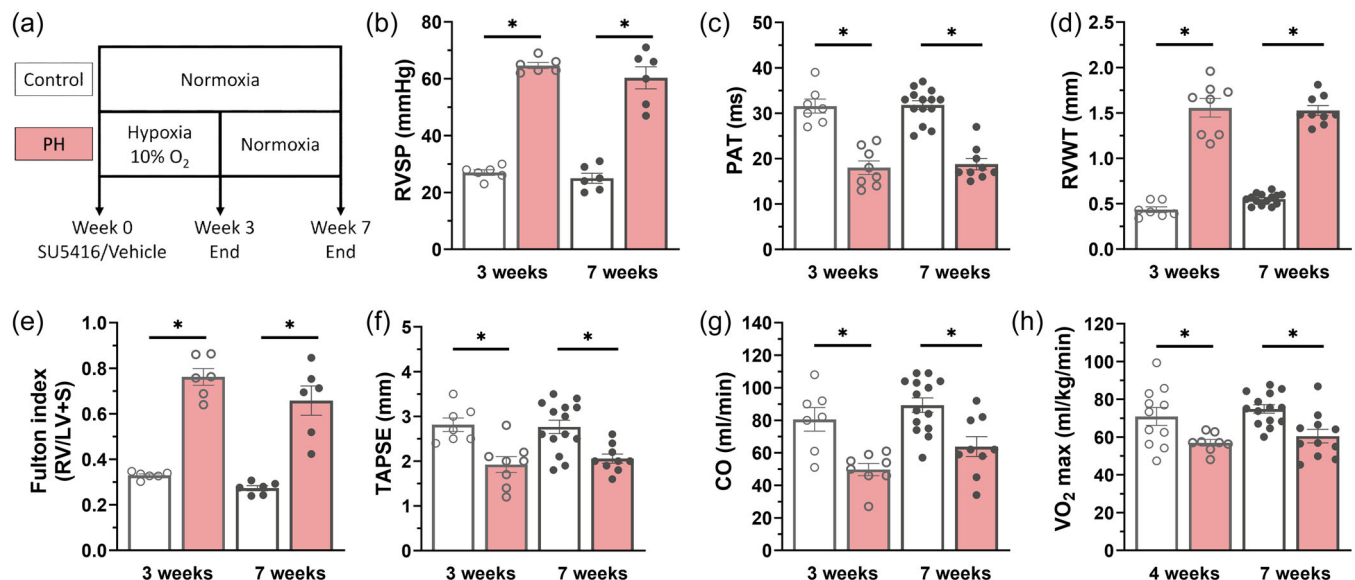


**FIGURE 1** Reduced exercise capacity is associated with RV dysfunction in PH SD rats. (a) Schematic of the experimental model of PH SD rats. PH was induced by a single subcutaneous injection of SU5416 and 3 weeks of normobaric hypoxia exposure, followed by housing at normoxic conditions for an additional 0–4 weeks. The control group (strain, age, and gender-matched rats) received a diluent injection and was housed in normoxic condition for the respective duration of the PH groups. Hemodynamic and echocardiographic measurements were performed at indicated timepoints, followed by tissue collection for ex vivo studies and biochemical analysis. (b) RVSP from hemodynamic measurement. Three and 7 weeks:  $n = 6$  control and  $n = 6$  PH. (c), (d), (f), and (g) Echocardiographic measurements of control and PH SD rats. Three weeks:  $n = 7$  control and  $n = 8$  PH; 7 weeks:  $n = 14$  control and  $n = 9$  PH. (e) Fulton index. Three and 7 weeks:  $n = 6$  control and  $n = 6$  PH. (h) Maximal aerobic capacity (VO<sub>2</sub> max) measured in control and PH SD rats. Please note that the VO<sub>2</sub> max was measured at the end of 4 weeks (instead of 3 weeks) in PH rats because of the required 1-week habituation after a full-term 3 weeks hypoxia exposure. Four weeks:  $n = 11$  control and  $n = 8$  PH; 7 weeks:  $n = 14$  control and  $n = 11$  PH. Mean  $\pm$  standard error of the mean. \* $p < 0.05$  for the indicated comparison. CO, cardiac output; LV, left ventricular; PAT, pulmonary acceleration time; PH, pulmonary hypertension; RV, right ventricular; RVSP, right ventricular systolic pressure; RVWT, right ventricular wall thickness; SD, Sprague–Dawley; TAPSE, tricuspid annular plane systolic excursion.

recorded in M-mode across the tricuspid valve annulus at the RV free wall and was determined by measuring the excursion of the tricuspid annulus from its highest position to the peak descent during ventricular systole. Tissue Doppler was used to measure the early diastolic velocity of the septum (at mitral annulus) and RV lateral wall (at tricuspid annulus).<sup>20</sup>

## VO<sub>2</sub> measurement

VO<sub>2</sub> measurement was performed as previously described<sup>21</sup> on a four-lane modular rodent treadmill (AccuPacer, Omnitech Electronics Inc.) equipped with individual metabolic chambers and a gas analyzer system that simultaneously monitors and records individual metabolic profiles (i.e., VO<sub>2</sub>, respiratory quotient, etc.) in real time. Before the test, animals were habituated to the treadmill through a gradual increase in running intensity to a final speed of 15 m/min at a 15° incline for 10 min/day.<sup>21</sup> The habituation phase occurred over a 1-week period and was used to assess running proficiency of individual animals,<sup>22,23</sup> while minimizing the potential for an aerobic training effect that can occur with longer habituation periods.<sup>24,25</sup> After the habituation period, a modified maximal exercise testing protocol<sup>26</sup> was used to determine exercise capacity (measured by maximal aerobic capacity; VO<sub>2</sub> max) using open-circuit spirometry (flow rate = 2–3 L/min) and consisted of incremental increases in speed and/or incline every 3–5 min. True VO<sub>2</sub> max was defined as (i) the point at which VO<sub>2</sub> does not change despite changes in workload during steady, consistent running, and (ii) a steady-state VO<sub>2</sub> that is sustained for a minimum of 1 min.

## Tissue collection

Animals were euthanized via exsanguination under anesthesia. Skeletal muscles were isolated and weighed, and either flash frozen in liquid nitrogen for histology, protein expression analysis, or immediately used for ex vivo force-frequency, fatigue analyses, and for mitochondrial respiration assays. The animals were randomly selected for different assays. The difference in numbers reflects the different processing of the tissue samples for the assays, as well as availability of tissue due to length of storage. All analyses were performed in a blind fashion.

## Fiber type composition assessments

Cryosections of skeletal muscle (5 μm) were blocked with 10% goat serum in phosphate-buffered saline (PBS), and

incubated with primary antibodies against myosin heavy chain Type I (1:50; BA-D5, Developmental Studies Hybridoma Bank [DSHB]), myosin heavy chain Type IIA (1:100; SC-71, DSHB), myosin heavy chain Type IIB (1:100; BF-F3, DSHB), myosin heavy chain Type IIX (1:100; 6H1, DSHB), and laminin (1:100; L9393, Sigma-Aldrich) for 1 h at room temperature, followed by appropriate IgG secondary antibodies for 1 h (Jackson ImmunoResearch). Image acquisition was performed on Zeiss LSM780 confocal microscope system. Quantification was performed using ImageJ software (National Institutes of Health, NIH). The total number of myofibers, fiber types, and cross-sectional area were semiautomatedly counted and quantified in the entire skeletal muscle cross-section using ImageJ software. Fiber types were expressed as percentage of total fibers. Cross-sectional area was expressed in μm<sup>2</sup>.

## Capillary density assessments

Cryosections of skeletal muscle (5 μm) were fixed with 4% paraformaldehyde, blocked with 10% goat serum in PBS, and incubated with primary antibodies against CD31 (1:100; MA1-81051, Thermo Fisher Scientific) and laminin (1:100; L9393, Sigma-Aldrich) for 1 h at room temperature, followed by appropriate secondary antibodies for 1 h (Jackson ImmunoResearch). Sections were also stained with Hoechst nuclear stain (33342, 1:1000 in PBS; Thermo Fisher Scientific). Image acquisition was performed on Zeiss LSM780 confocal microscope system. Quantification was performed using ImageJ software (NIH). The total number of positive CD31 nuclei were semiautomatedly counted in three different regions of soleus cross-section using ImageJ software.

## Muscle fiber preparation and mitochondrial respiratory function assessments

Immediately after euthanasia, a small muscle biopsy from soleus tissue was placed in ice-cold relaxing and biopsy preservation solution (BIOPS, pH7.1) containing (in mM) 2.77 CaK<sub>2</sub>EGTA, 7.23 K<sub>2</sub>EGTA, 5.77 Na<sub>2</sub>ATP, 6.56 MgCl<sub>2</sub>·6H<sub>2</sub>O, 20 Taurine, 15 Na<sub>2</sub> Phosphocreatine, 20 Imidazole, 0.5 Dithiothreitol, 50 MES hydrate; pH 7.1). Using a dissecting microscope, connective tissue was removed and muscle fiber bundles were separated mechanically with sharp angular forceps over a standardized period of 3 min while submerged in ice-cold BIOPS. Separated muscle fibers were then permeabilized with 50 μg/mL saponin in BIOPS for 30 min at 4°C with

gentle agitation, followed by transfer of the muscle fibers into ice-cold respiration buffer MiR05 (in mM: 0.5 EGTA, 3 MgCl<sub>2</sub>·6H<sub>2</sub>O, 60 lactobionic acid, 20 taurine, 10 KH<sub>2</sub>PO<sub>4</sub>, 20 HEPES, 110 D-Sucrose, and 1 g/L fatty acid-free bovine serum albumin; pH 7.1) for 10 min with gentle agitation at 4°C. After quickly blotting dry and measurement of wet weight using a microbalance, 1–2 mg of permeabilized muscle fibers were transferred into high-resolution O2k respirometer chambers (Oroboros Instruments) filled with MiR05 respiration buffer containing 280 U/mL catalase at 37°C for mitochondrial respiratory function analysis. Respiratory states were induced using substrate–uncoupler–inhibitor titration (SUIT) protocol by stepwise addition of pyruvate (5 mM) and malate (2 mM), adenosine diphosphate (ADP, 7.5 mM), carbonyl cyanide *p*-trifluoromethoxyphenylhydrazone (FCCP, 0.05 μM stepwise titration to reach maximal respiration), succinate (10 mM), rotenone (0.5 μM), and antimycin-A (2.5 μM). Permeabilized muscle fibers from each animal were analyzed in duplicate. Oxygen concentration was maintained above 200 μM throughout the experiment to avoid limitations in oxygen supply. To keep the closed-chamber system, reoxygenation during the experiment was performed by injection of a small amount of hydrogen peroxide. Oxygen flux rates were normalized per milligram of tissue wet weight.

### Ex vivo force-frequency and fatigue assessments

Ex vivo characteristics of intact skeletal muscle were performed as previously described.<sup>27</sup> Whole isolated muscle was ligated at both ends and bathed in Krebs Buffer (in mM: 118 NaCl, 4.7 KCl, 2.5 CaCl<sub>2</sub>, 1.7 MgSO<sub>4</sub>, 24.9 NaHCO<sub>3</sub>, six glucose, two sodium pyruvate) supplied with a mixture of oxygen (95%) and CO<sub>2</sub> (5%). Contractile forces were generated by electrical stimulation from a Grass stimulator and detected using a force transducer that was integrated with an ADI PowerLab system and LabChart 8 Pro software.<sup>28</sup> Voltage was determined by assessing maximal twitch response to increasing voltages and used for subsequent tetanic stimuli. For force-frequency protocol, muscle was stimulated with incremental stimulation frequencies (1, 10, 20, 30, 40, 50, 70, 100, and 150 Hz). Stimuli were applied with a train duration of 300 ms. The resting interval was 30 s between the stimulations at 1 and 10 Hz; 60 s after stimulation at 20 Hz; 90 s after stimulation at 30 Hz; and 120 s between stimulations at 50, 70, 100, and 150 Hz. For the fatigue protocol, muscle was stimulated at the frequency associated with ½ maximal force stimulation, with 300 ms duration every 3 s for 5 min. At the end of

the protocols, the length and weight of muscle were determined. Force (in N/cm<sup>2</sup>) was normalized to muscle cross-sectional area (in cm<sup>2</sup>), which was calculated by dividing muscle weight (g) by muscle length (cm) multiplied by specific density 1.056 g/mL.

### Western blot analysis

Skeletal muscles were homogenized at 4°C in RIPA buffer supplemented with Pierce protease inhibitor (Thermo Fisher Scientific) and phosphatase inhibitors (Boston BioProducts) using the Tissue Lyser II (Qiagen). Homogenates were centrifuged at 2500 × g at 4°C for 10 min. The resulting supernatant was collected for protein analysis. Protein concentration was determined with Pierce BCA Protein Assay Kit (Thermo Fisher Scientific). Equal amounts of proteins were separated by sodium dodecyl-sulfate polyacrylamide gel electrophoresis, transferred to polyvinylidene fluoride or nitrocellulose membranes, immunoblotted, and visualized and quantified using Bio-Rad Imager Chemidoc. The following primary antibodies and respective dilutions were used with overnight incubation at 4°C: pAMPKα (1:1000; #2535, Cell Signaling), AMPKα (1:1000; #5832, Cell Signaling), PGC1-α (1:1000, sc-13067, Santa Cruz Biotechnology), DRP1 (1:500; sc-32898, Santa Cruz), Pink1 (1:1000; sc-33796, Santa Cruz), Vinculin (1:3000; #V9131, Sigma Aldrich). Vinculin was used as loading control protein.

### Mitochondrial DNA (mtDNA) content

Total DNA was extracted using DNeasy Blood and Tissue Kit (Qiagen). Real-time polymerase chain reaction (PCR) was performed using the SsoAdvanced Universal SYBR Green Supermix (Bio-Rad) and Step One Plus Real-time PCR System (Applied Biosystems) for Cytochrome b (mtDNA, For: GCCCAATCACCCAAACTCTA, Rev: TACTGGTTGGCCTCCAATTC). Skeletal α-actin (For: GTCGGTATGGGTCAGAAGGA, Rev: TGTCGTCCCAG TTGGTGATA) was used for nuclear DNA. Each sample was assayed in duplicate in two independent PCR reactions. Samples without a template served as negative controls. Cytochrome b levels were normalized to skeletal α-actin DNA for relative expression in each sample.

### Statistical analysis

All data are presented as mean ± standard error of the mean. Statistical differences were assessed by unpaired,

two-tailed Student's *t* test, one-way analysis of variance (ANOVA) followed by Bonferroni posttests for comparison of individual means, or two-way ANOVA followed by Turkey's multiple comparison test. A *p* value of <0.05 was considered statistically significant.

## RESULTS

### Reduced exercise capacity in PH SD rats

We first investigated exercise capacity in PH SD rat model. As shown in Figure 1a, two timepoints were selected: 3 weeks (immediately after hypoxia) and 7 weeks (3 weeks of hypoxia and then 4 weeks of normoxia) after SU5416 injection. Compared to the control rats, the PH SD rats showed a 2.4-fold increase in RVSP (Figure 1b) and a 41%–43% reduction in PAT (Figure 1c and Supporting Information S1: Figure 1) at 3- and 7-week timepoints. The PH SD rats developed RV hypertrophy with increased RV free wall thickness (Figure 1d) and Fulton index (Figure 1e) together with RV systolic dysfunction indicated by reduced TAPSE (Figure 1f and Supporting Information S1: Figure 1) and CO (Figure 1g) at 3-week timepoint, which continued at 7-week timepoint. In parallel to the development of PH and RV dysfunction, the PH SD rats had a significant reduction in maximum oxygen uptake ( $\text{VO}_2$  max; Figure 1h) compared to the control rats via exercise testing.

### PH SD rats show skeletal muscle fiber type switching at 3-week timepoint but not 7-week timepoint

To determine whether there are changes in muscle structure, we performed histological analysis to assess muscle atrophy, fiber type switching, and capillary density in soleus muscles. Figure 2a shows the representative images of soleus muscles stained for myosin heavy chain (MHC) Type I, MHC Type IIA, and laminin (stain for cell membrane) from the control and PH SD rats at both 3 weeks and 7-week timepoints. Our quantitated data demonstrated no changes in muscle mass (Figure 2b), cross-sectional areas of the muscle fiber Type I (Figure 2c), or cross-sectional areas of the muscle fiber Type IIA (Figure 2d). In contrast, our data showed fiber type switching, evidenced by a decrease in the muscle fiber Type I composition (Figure 2e) and an increase in the muscle fiber Type IIA composition (Figure 2f) in the PH SD rats at 3-week timepoint. These changes were no longer

present at the 7-week timepoint. Similar findings were found for capillary density showing a reduction in the PH SD rats at 3-week timepoint but not at 7-week timepoint (Figure 2g,h).

### No changes in skeletal muscle mitochondrial function, isometric force, or fatigue profile in PH SD rats

Mitochondria play a critical role in metabolic regulation and ATP production that are directly related to skeletal muscle contractility and plasticity. Therefore, we assessed mitochondrial respiration in soleus muscle fibers using high-resolution O2K Respirometer (Oroboros).<sup>29</sup> As shown in Figure 3a,  $\text{O}_2$  consumption was measured in permeabilized soleus muscle fibers from control and PH rats to determine mitochondrial complex I (CI)- and CII-linked respiration (pyruvate/malate as CI substrates and succinate as CII substrate). ADP was used to induce CI-linked oxidative phosphorylation (OXPHOS), while FCCP was used to induce the maximum electron transfer capacity. Our data showed that there were no changes in  $\text{O}_2$  consumption in the soleus muscle fibers of the PH SD rats compared to the control rats at both 3-week (Figure 3b,  $p = 0.63$ – $0.77$  for the effects of PH on different measures) and 7-week timepoints (Figure 3c,  $p = 0.37$ – $0.77$  for the effects of PH on different measures), suggesting no changes in intrinsic mitochondrial function between the control and PH SD rats in our experimental period, despite a reduction in the exercise capacity in these animals. In addition, no change was noted in mitochondrial DNA content in soleus muscle fibers between the control and PH SD rats (Figure 3d).

Next, we measured isometric force and fatigue profile in soleus muscle *ex vivo* at 7-week timepoint. Intact soleus muscle fibers were isolated, bathed in a solution supplied with sufficient metabolism substrates and oxygen, and stimulated by electrical stimulations. Because this approach removes the nerve and blood supply and focuses on the isolated skeletal muscle itself, it allows direct assessment of the intrinsic properties of the skeletal muscle. Interestingly, while the PH SD rats showed a reduction in exercise capacity, there were no changes in isometric force-frequency relationship (Figure 3e,  $p = 0.87$  for the effects of PH) or fatigue profiles (Figure 3f,  $p = 0.17$  for the effects of PH) in soleus muscles of the control and PH rats, suggesting same intrinsic contractile properties of the soleus muscles between the two groups. Consistently, there were no changes in proteins (i.e., pAMPK, PGC1 $\alpha$ , DRP1, PINK1) that are involved in metabolism and mitochondrial regulation (Figure 4).

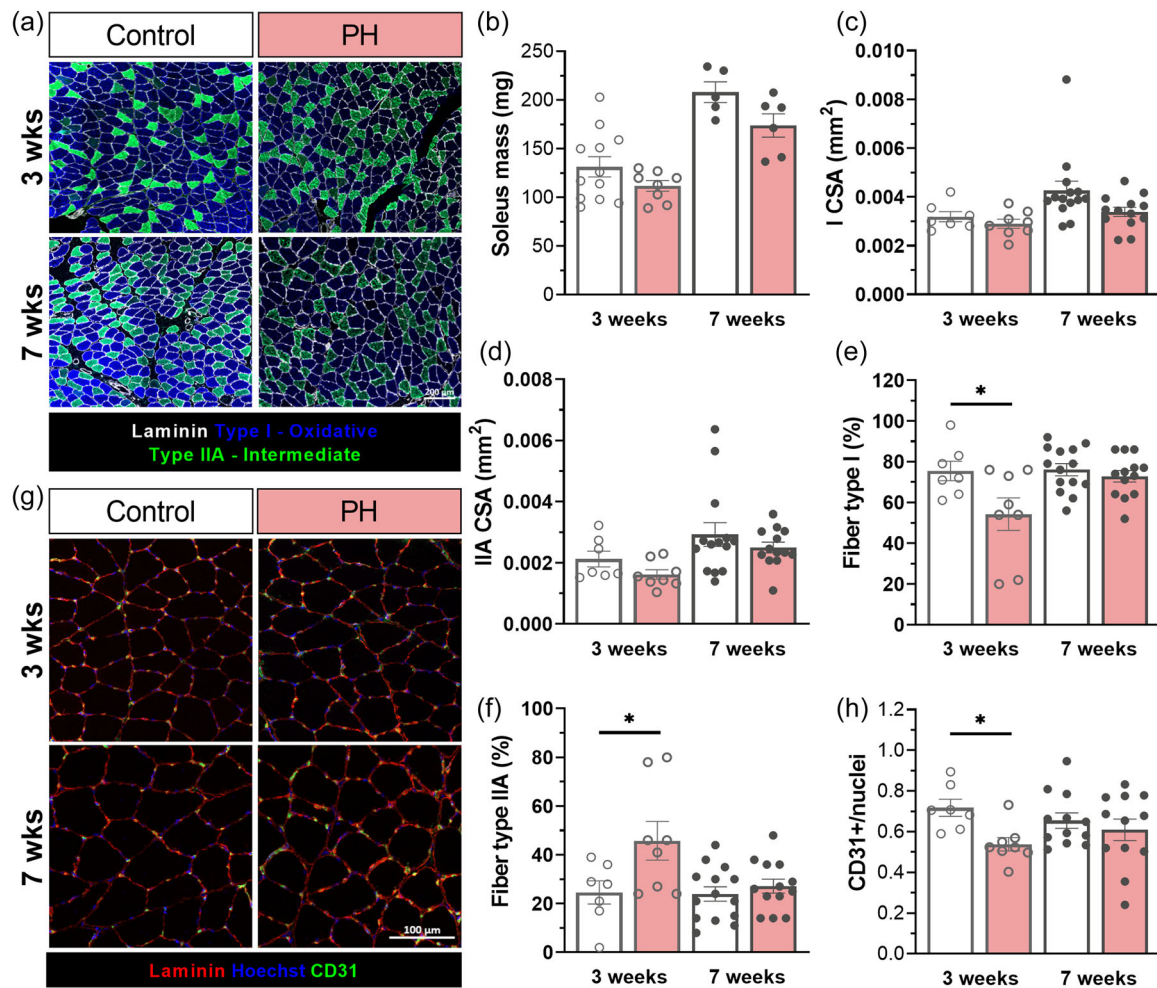


**FIGURE 2** PH SD rats show solues muscle fiber type switching and capillary density reduction at 3-week timepoint but not 7-week timepoint. (a) Representative confocal images of soleus muscles stained for MHC Type I (blue), MHC Type IIA (green), and laminin (white). Scale bar: 200  $\mu\text{m}$ . (b) Quantitated soleus muscle mass. Three weeks:  $n = 12$  control and  $n = 8$  PH; 7 weeks:  $n = 5$  control and  $n = 6$  PH. (c) Quantitated cross-sectional area of the Type I muscle fiber (I CSA). (d) Quantitated cross-sectional area of the Type IIA muscle fiber (IIA CSA). (e) Quantitated percentage of Type I muscle fiber composition. (f) Quantitated percentage of Type IIA muscle fiber composition. In (c)–(f), 3 weeks:  $n = 7$  control and  $n = 8$  PH; 7 weeks:  $n = 14$  control and  $n = 13$  PH. (g) Representative confocal images of soleus muscles stained for CD31 (green), laminin (red), and nuclei (Hoechst, blue). Scale bar: 100  $\mu\text{m}$ . (h) Quantitated data from (h) showing CD31 positive cells in total cells. Three weeks:  $n = 7$  control and  $n = 8$  PH; 7 weeks:  $n = 12$  control and  $n = 12$  PH. Mean  $\pm$  standard error of the mean. \* $p < 0.05$  for the indicated comparison. MHC, myosin heavy chain; PH, pulmonary hypertension; SD, Sprague–Dawley.

### Reduced exercise capacity in PH CDF rat model, a more severe PH model

Since we observed little intrinsic changes in soleus muscle in the PH SD rat model and the occurrence of intrinsic changes in soleus muscle is likely to be related with the severity of PH, we next determined the exercise capacity and the structural and functional changes in soleus muscles using SuHx-induced PH model in Fischer rats (PH CDF rats). We and others have demonstrated that the PH CDF rats have a more severe PH phenotypes than the PH SD rats.<sup>19,30</sup> It is noted that the PH CDF rats start to die in Week 5 after

initiation of the PH induction by SU5416 injection. Therefore, we performed the studies at the end of Week 4, which consists of 3 weeks of hypoxia and 1 week of normoxia after SU5416 injection (Figure 5a). CDF rats injected with vehicle and kept at normoxia for the course of the experiments were used as controls. The PH CDF rats showed a 3.7-fold increase in RVSP (Figure 5b) and a 59% reduction in PAT (Figure 5c and Supplemental Figure 1) compared to the control rats, which is associated with RV hypertrophy (Figure 5d,e), RV systolic dysfunction (Figure 5f,g and Supporting Information S1: Figure 1), and reduced exercise capacity (Figure 5h).

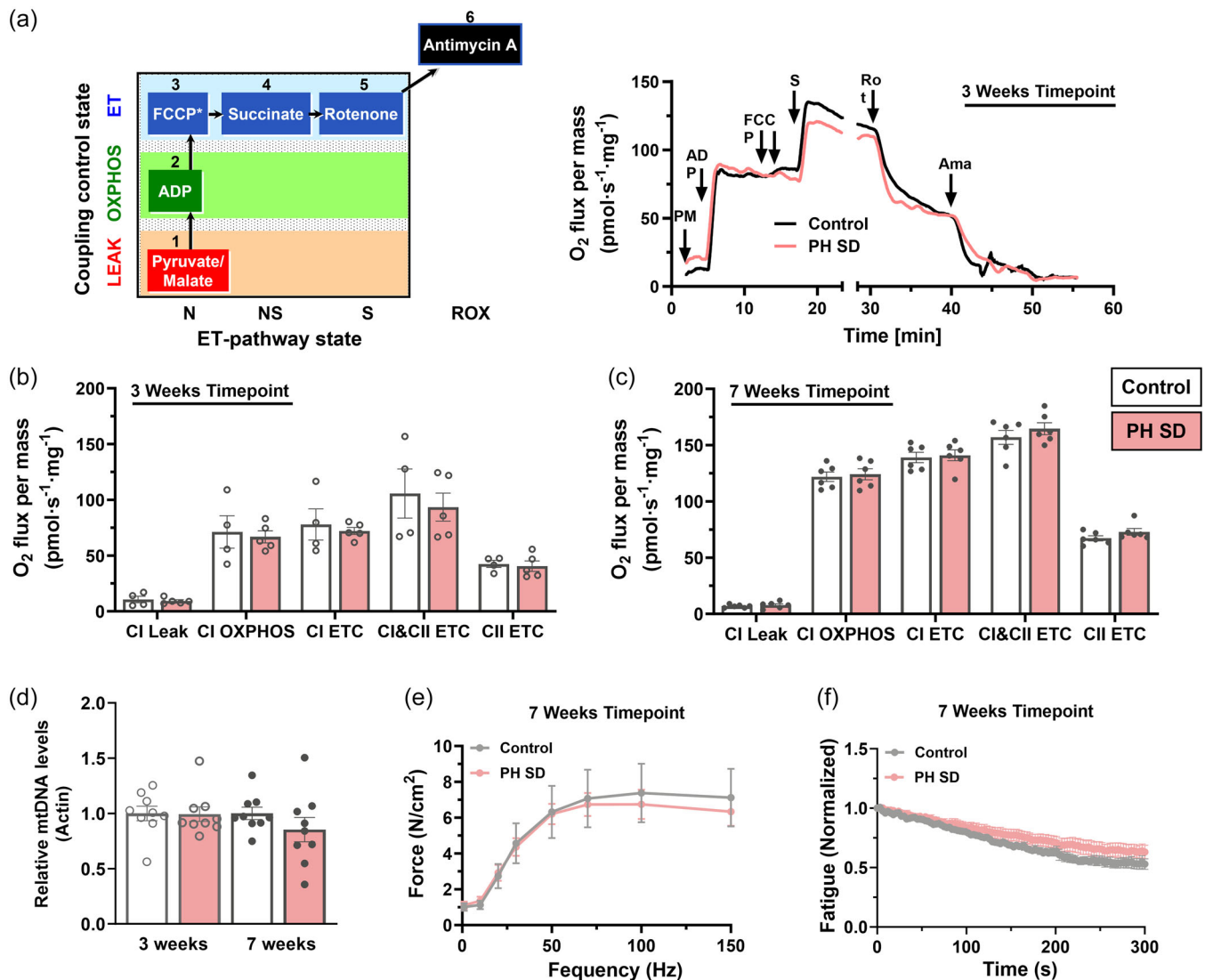


**FIGURE 3** No changes in soleus muscle mitochondrial function, isometric force, or fatigue profile in PH SD rats. (a) Mitochondrial respiration measurements in permeabilized soleus muscle fibers using Oroboros. (Left) SUIIT protocol used. (Right) Representative tissue mass-specific oxygen flux traces recorded in control and PH SD rats. Sequential addition of pyruvate and malate (PM), ADP, FCCP, succinate (S), rotenone (Rot) yields CI-linked, CI and CII-linked, and CII-linked respiration. Residual oxygen consumption (ROX) recorded after adding Antimycin A (Ama). (b) and (c) Quantitated data of mitochondrial respiration from 3-week timepoint (b,  $n = 4$  control and  $n = 5$  PH,  $p = 0.63$ – $0.77$  for the effects of PH on different measures) and 7-week timepoint (c,  $n = 6$  control and  $n = 6$  PH,  $p = 0.37$ – $0.77$  for the effects of PH on different measures). (d) Relative mitochondrial DNA level (quantitative reverse transcription polymerase chain reaction) normalized to Skeletal  $\alpha$ -actin and expressed relative to controls.  $n = 9$  per group. (e) and (f) Quantitated data of isometric force-relationship (e,  $n = 6$  per group,  $p = 0.87$  for the effects of PH) and fatigue profile (f,  $n = 5$  per group,  $p = 0.17$  for the effects of PH) by ex vivo force-frequency and fatigue assessments. Mean  $\pm$  standard error of the mean. ADP, adenosine diphosphate; ETC, electron transfer capacity; FCCP, carbonyl cyanide *p*-trifluoromethoxyphenylhydrazone; N, NADH-linked pathway state; NS, NADH-linked and succinate pathway state; OXPHOS, oxidative phosphorylation; PH, pulmonary hypertension; S, succinate pathway state; SD, Sprague–Dawley.

### Skeletal muscle in PH CDF rats shows atrophy at 4-week timepoint

Similar to the assessments in the PH SD rats, we performed histological analysis to assess structure changes in soleus muscle, including muscle atrophy, fiber type switching, and capillary density (Figure 6). Compared to

the control rats, the PH CDF rats showed soleus muscle atrophy that was indicated by a 15% reduction in muscle mass (Figure 6b), a 37% reduction in cross-sectional areas of the Type I muscle fiber (Figure 6c), and a 27% reduction in cross-sectional areas of the Type IIA muscle fiber (Figure 6d), although there were no changes in fiber type composition (Figure 6e,f) or capillary density (Figure 6g,h)

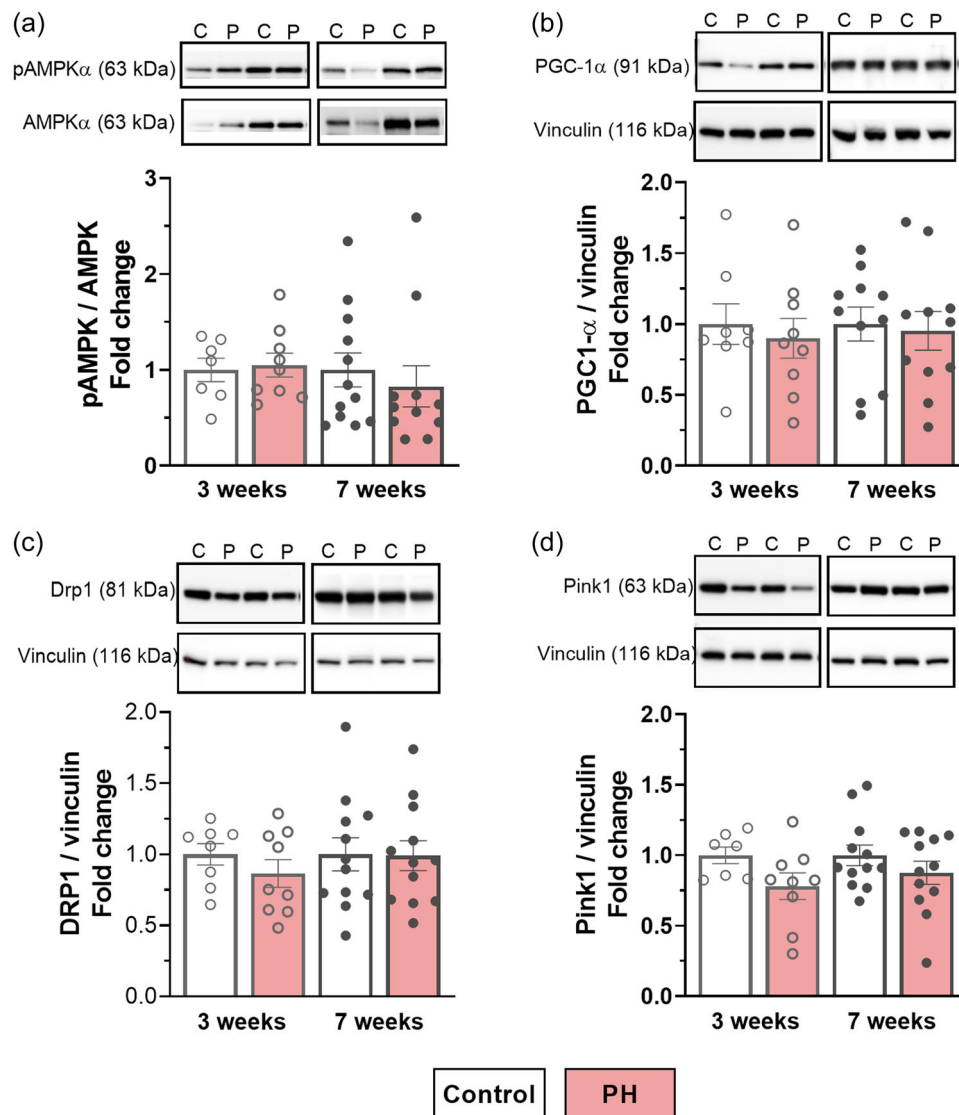


**FIGURE 4** No changes in proteins involved in metabolism and mitochondrial regulation in soleus muscle of control and PH SD rats. Western blots were performed using soleus muscle lysates from control and PH SD rats at 3- and 7-week timepoints. Representative immunoblots (top; c: control, P: PH) and quantitative analysis (bottom) of relative expression of (a) phospho-AMPK $\alpha$  (pAMPK $\alpha$ )/total AMPK $\alpha$  (AMPK $\alpha$ ) ratio, (b) peroxisome proliferator-activated receptor- $\gamma$  coactivator (PGC-1 $\alpha$ ); (c) dynamin-related protein 1 (DRP1); (D) PTEN-induced kinase 1 (Pink1). Data were normalized to vinculin (loading control) and expressed relative to respective controls of the timepoints. Three weeks:  $n = 7-9$  per group; 7 weeks:  $n = 11-12$  per group. Mean  $\pm$  standard error of the mean. PH, pulmonary hypertension; SD, Sprague-Dawley.

in soleus muscles between the control and PH CDF rats. To determine whether these observed changes are unique in soleus muscles predominantly containing Type I muscle fibers, we then assessed muscle mass and structure changes (cross-sectional areas and fiber types) in EDL muscles that predominantly contain Type II muscle fibers. As shown in Supporting Information S1: Figure 2a, the EDL muscles in the PH CDF rats have a 10% reduction in muscle mass and a trend 17% reduction ( $p = 0.12$ ) in Type I fibers, but lack of changes in cross-sectional areas of Type I fiber or any changes in various Type II (IIA, IIB, and IIX) fibers, indicating a similar atrophy but less

structural changes in EDL muscles than soleus muscles in PH CDF rats.

### No changes in skeletal muscle mitochondrial function, force, or fatigue profile in PH CDF rats despite altered expression of metabolism and mitochondrial related signaling proteins

We then performed the measurements using high-resolution O2K Respirometer with the same protocol

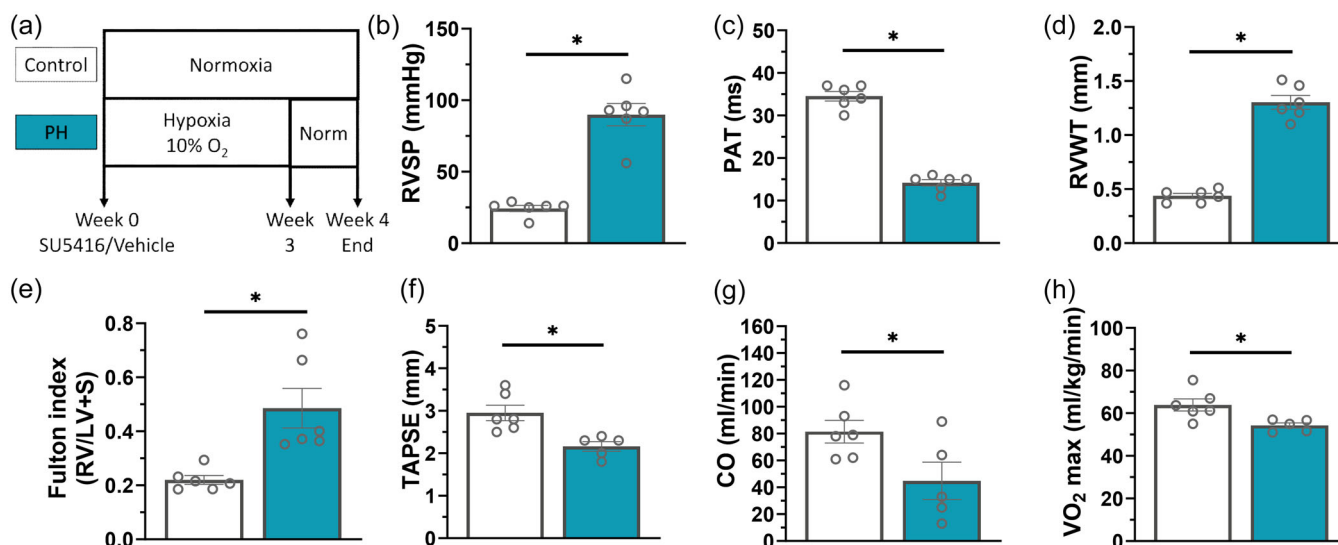


**FIGURE 5** Reduced exercise capacity is associated with right ventricular dysfunction in PH CDF rats. (a) Schematic of the experimental model of PH CDF rats. PH was induced by a single subcutaneous injection of SU5416 and 3 weeks of normobaric hypoxia exposure, followed by housing at normoxic conditions for an additional 1 week. The control group (strain, age, and gender-matched rats) received a diluent injection and was housed in normoxic condition for 4 weeks. Hemodynamic and echocardiographic measurements were performed at the end of 4 weeks, followed by tissue collection for ex vivo studies and biochemical analysis. (b) Right ventricular systolic pressure from hemodynamic measurement. (c), (d), (f), and (g) Echocardiographic measurements of control and PH CDF rats. (e) Fulton index. (h) Maximal aerobic capacity ( $VO_2$  max) measured in control and PH CDF rats at the end of 4 weeks.  $n = 6$  control and  $n = 5-6$  PH. Mean  $\pm$  standard error of the mean. \* $p < 0.05$  for the indicated comparison. CDF, Fischer rats; CO, cardiac output; PAT, pulmonary acceleration time; PH, pulmonary hypertension; RVWT, right ventricular wall thickness; SD, SD, Sprague–Dawley; TAPSE, tricuspid annular plane systolic excursion.

outlined in Figure 3a to assess mitochondrial respiration in soleus muscle fibers of control and PH CDF rats. Despite the severe PH phenotypes in PH CDF rats, there are no changes in  $O_2$  consumption in the soleus muscle fibers of PH CDF rats compared to control rats (Figure 7a,  $p = 0.28-0.82$  for the effects of PH on different measures), suggesting no changes in intrinsic mitochondrial function between the control and PH CDF rats. Also, there was no change in mitochondrial DNA content in soleus muscle fibers between control and PH CDF rats (Figure 7b). We also found no changes in isometric force-frequency relation ( $p = 0.80$  for the effects of PH) or fatigue profile ( $p = 0.35$  for the effects of PH on different measures) in soleus muscle (Figure 7c,d) between control and PH CDF rats, suggesting same intrinsic properties of the soleus muscles. Similarly, we assessed mitochondrial respiration and fatigue profile in EDL muscle. As expected, the  $O_2$  consumption in the EDL muscle fibers (Supporting Information S1: Figure 2b) is lower than that in soleus muscle fibers (Figure 7a), because of the high abundance of Type I muscle fibers in soleus muscles that have a distinct metabolic phenotype. Our data further showed that EDL muscles have comparable mitochondrial function ( $p = 0.24-0.90$  for the effects of PH on different measures) and fatigue profile ( $p = 0.25$  for the

effects of PH) in the control and PH CDF rats (Supporting Information S1: Figure 2b,c).

Using soleus muscle lysates, we also performed Western Blot for proteins that are involved in metabolism and mitochondrial regulation and found some changes in the signaling related to metabolism and mitochondrial regulation (Figure 8), including an increase in pAMPK (metabolic sensors) and PGC1 $\alpha$  (regulator of mitochondrial biogenesis) and a decrease in DRP1 and PINK1 (regulators of mitochondrial fission).

## DISCUSSION

In this study, we performed a comprehensive evaluation of intrinsic changes in soleus and EDL muscles using contemporary SuHx rat PH model in two strains showing reduced exercise capacity with different PH severity. Our data shows that there was a lack of alteration in skeletal muscle morphology, structure, isometric force and fatigue profile, or mitochondrial respiration in PH SD rats, despite presence of PH, RV dysfunction, and impaired exercise capacity. In the PH CDF rats that have more severe PH, soleus muscle showed atrophy together with altered intracellular signal transduction

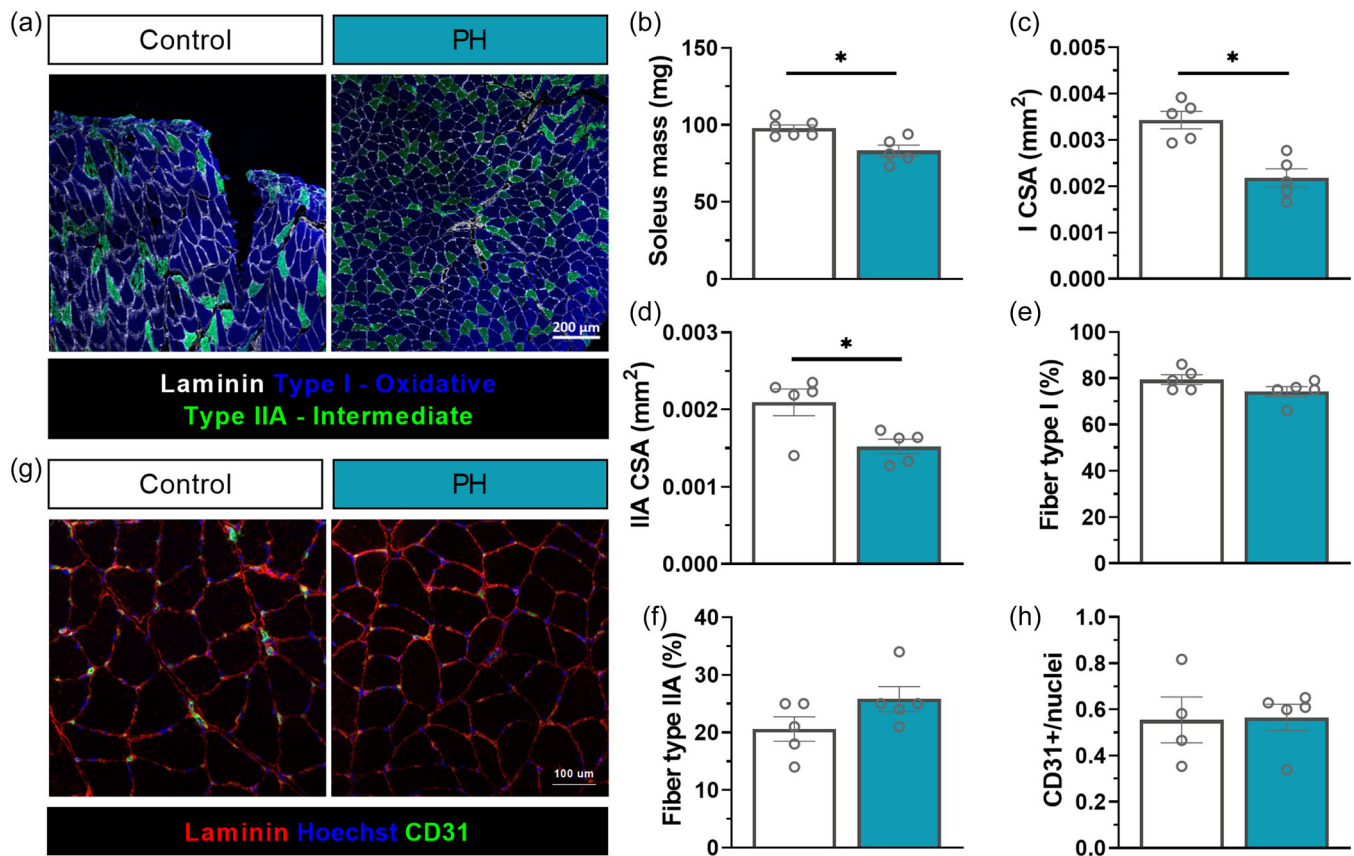


**FIGURE 6** PH CDF rats show soleus muscle atrophy at 4-week timepoint. (a) Representative confocal images of soleus muscles stained for MHC Type I (blue), MHC Type IIA (green), and laminin (white). Scale bar: 100  $\mu$ m. (b) Quantitated soleus muscle mass.  $n = 6$  control and  $n = 5$  PH. (c) Quantitated cross-sectional area of the Type I muscle fiber (I CSA). (d) Quantitated cross-sectional area of the Type IIA muscle fiber (IIA CSA). (e) Quantitated percentage of Type I muscle fiber composition. (f) Quantitated percentage of Type IIA muscle fiber composition. In (c)–(f),  $n = 5$  control and  $n = 5$  PH. (g) Representative confocal images of soleus muscles stained for CD31 (green), laminin (red), and nuclei (Hoechst, blue). Scale bar: 100  $\mu$ m. (h) Quantitated data from (h) showing CD31 positive cells in total cells.  $n = 4$  control and  $n = 5$  PH. Mean  $\pm$  standard error of the mean. \* $p < 0.05$  for the indicated comparison. CDF, Fischer rats; MHC, myosin heavy chain; PH, pulmonary hypertension.

related to metabolism and mitochondrial regulation, but functional parameters including muscle mitochondrial function, isometric force, and fatigue profile remain unchanged. Similarly, the EDL muscles in the PH CDF rats also showed atrophy but lack of functional changes in mitochondrial respiration and fatigue profile. These data demonstrate that reduced exercise capacity in PH occurs before intrinsic dysfunction in skeletal muscle in SuHx-induced PH rat model, which strongly suggests that intrinsic alterations in skeletal muscle are not causative to exercise intolerance in PH.

PH develops in response to the progressive loss and remodeling of the pulmonary vessels, and results in right heart dysfunction, failure, and death. Despite new therapies, most patients with PH display persistent exercise intolerance, which significantly impact patients' quality of life.<sup>6</sup> Measures of exercise intolerance such as  $VO_2$  max and distance walked in 6 min are

routinely used to prognosticate patients with PH and follow response to treatment. Moreover, the reduction in the  $VO_2$  max is a better predictor of mortality than the central hemodynamic deficit or other traditional risk factors.<sup>31</sup> Preclinical animal models have been used to help understand the pathophysiological process of PH and the underlying mechanisms. Among them, the monocrotaline (MCT)- and the SuHx-induced PH rat models are the two main models used in PH with different pathophysiological characteristics: the MCT-induced PH rat model is associated with endothelial toxicity and marked lung inflammation, while SuHx-induced PH rat model is characterized by pulmonary vascular proliferative lesions such as the formation of neointimal plexiform lesions.<sup>32,33</sup> Although the MCT PH model has long been used in many studies, including studies of exercise capacity in PH,<sup>12,14,34–36</sup> MCT-induced broad toxicity and severe inflammation in multiple

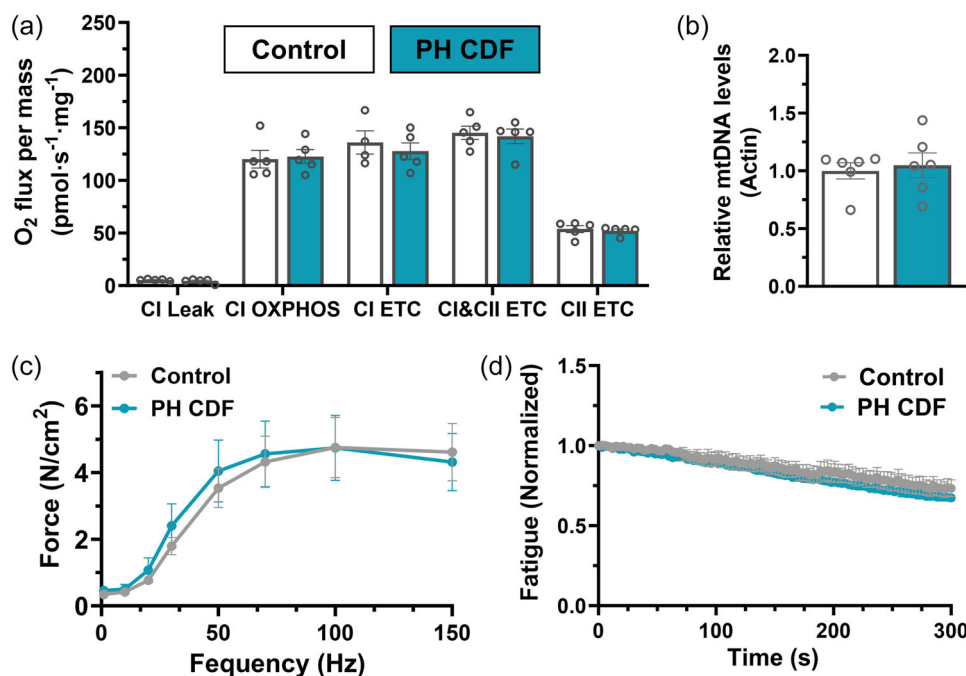


**FIGURE 7** No changes in soleus muscle mitochondrial function, isometric force, or fatigue profile in PH CDF rats. (a) Quantitated data of mitochondrial respiration from control and PH CDF rats at 4-week timepoint.  $n = 5$  per group.  $p = 0.28$ – $0.82$  for the effects of PH on different measures. (b) Relative mitochondrial DNA level (quantitative reverse transcription polymerase chain reaction) normalized to Skeletal  $\alpha$ -actin and expressed relative to controls.  $n = 6$  per group. (c) and (d) Quantitated data of ex vivo isometric force–frequency relationship ( $p = 0.80$  for the effects of PH) and fatigue profile ( $p = 0.35$  for the effects of PH).  $n = 6$  control and 4 PH. Mean  $\pm$  standard error of the mean. CDF, Fischer rats; ETC, electron transfer capacity; OXPHOS, oxidative phosphorylation; PH, pulmonary hypertension.

organs<sup>32,33</sup> add significant confounding effects that may be independent of PH. In addition, the MCT-induced very high mortality also limits its usage in studying PH progression. In this study, we used the SuHx rat model, a contemporary model of PH that recapitulates the pathological lesions present in the lungs of PH patients,<sup>32</sup> to study the changes in skeletal muscle and their relationship to the exercise intolerance in PH. Moreover, we took advantage of the different PH severity due to rat strains in SuHx model and used two rat strains: the PH CDF rats develop a more severe PH phenotype associated with high mortality after 5 weeks, while the PH SD rats have good survival up to 14 weeks. Our data (Figures 1c and 5c) showed that the PAT was reduced by 41%–43% in PH SD rats and by 59% in the PH CDF rats (compared to their respective controls), suggesting higher pulmonary artery pressure in the PH CDF rats than the PH SD rats, which is consistent with our observation that the PH CDF rats develop higher RVSP (PH CDF 90 mmHg vs. PH SD 60–65 mmHg, Figures 1b and 5b) and worse RV maladaptation than the PH SD rats.<sup>19</sup> While the mechanisms underlying the differences in PH severity between SD and CDF rats warrant further investigations, our data suggest that higher PVR and RVSP in PH CDF rats may be a major driving force. In addition, the high

mortality in the PH CDF model is believed to be caused by a failure of RV adaptation associated with lack of adequate microvascular angiogenesis, together with metabolic and immunological responses in the hypertrophied RV.<sup>30,37</sup> Therefore, using the SuHx-induced PH model in two rat strains and different timepoints (i.e., 3 weeks and 7 weeks for SD rats and 4 weeks for CDF rats), we were able to evaluate the relationship between exercise capacity and intrinsic changes in peripheral skeletal muscle during the development of PH and with variable PH severity. Our data showed that reduced exercise capacity occurred in all three PH scenarios, which is consistent with findings from PH patients and other preclinical PH animal models, and all these studies confirm that impaired exercise capacity is a common feature in PH.

To date, several mechanisms have been postulated to explain the reduced exercise capacity in PH. Notably, exercise requires the interaction of several physiological mechanisms. In addition to intrinsic mass and function of skeletal muscles, both respiratory and cardiovascular systems have to be coupled to meet the metabolic demands of the contracting skeletal muscles. Therefore, central cardiopulmonary impairments in PH have long been viewed as primary factors resulting in exercise

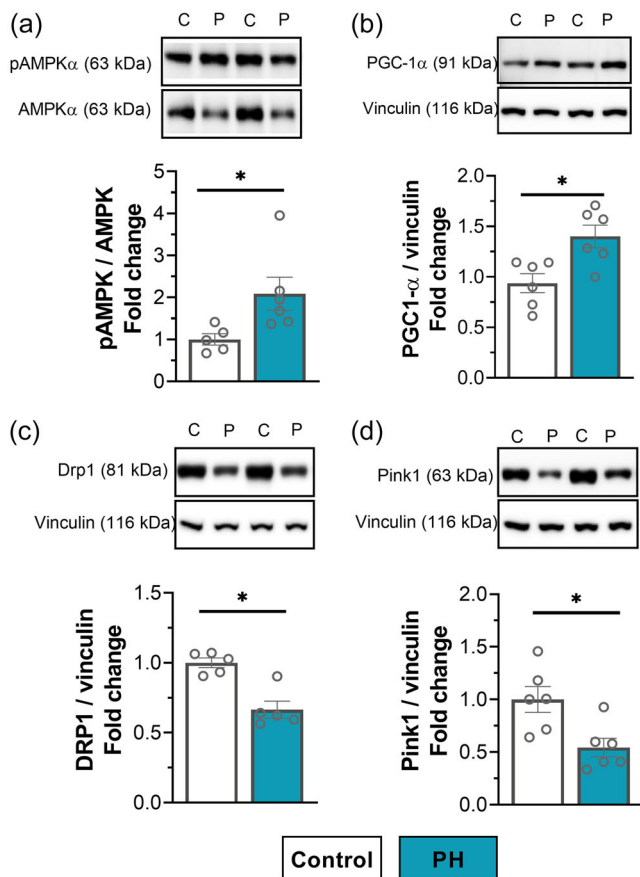


**FIGURE 8** Soleus muscles of PH CDF rats at 4-week timepoints show changes in proteins involved in metabolism and mitochondrial regulation. Western blots were performed using soleus muscle lysates from control and PH CDF rats at 4-week timepoints. Representative immunoblots (top; c: control, P: PH) and quantitative analysis (bottom) of relative expression of (a) phospho-AMPK $\alpha$  (pAMPK $\alpha$ )/total AMPK $\alpha$  (AMPK $\alpha$ ) ratio, (b) Peroxisome proliferator-activated receptor- $\gamma$  coactivator (PGC-1 $\alpha$ ); (c) dynamin-related protein 1 (DRP1); (d) PTEN-induced kinase 1 (Pink1). Data were normalized to vinculin (loading control) and expressed relative to controls.  $n = 5-6$  per group. Mean  $\pm$  standard error of the mean, \* $p < 0.05$  for the indicated comparison. CDF, Fischer rats; PH, pulmonary hypertension.

intolerance in patients with PH. Indeed, a meta-analysis of 16 randomized trials including 2353 patients with pulmonary arterial hypertension showed that changes in cardiac index significantly correlated with changes in exercise capacity.<sup>38</sup> The results of our study support this mechanism because reduced exercise capacity in our SuHx-induced PH rat model in two strains with different severity was associated with RV systolic dysfunction and significant reduction in cardiac output, regardless of whether there were intrinsic changes in skeletal muscle or not.

In addition to the central cardiopulmonary impairments that co-exist with reduced exercise capacity in PH

patients and animal models, changes were also observed in skeletal muscles including skeletal muscle atrophy and impaired force generation,<sup>9,13,39,40</sup> lower proportion of Type I muscle fibers,<sup>39,40</sup> or reduced capillary density,<sup>41</sup> suggesting that intrinsic changes in skeletal muscles also occur in PH and can contribute to impaired exercise capacity. However, these observations were not consistently detected in all studies, that is, certain alterations were detected in some studies but not others. In this study, we did observe some changes in the distribution of Type I and Type II muscle fibers and in capillary density in soleus muscle at the 3-week timepoint in the PH SD rat model. However, these alterations were no longer present at the 7-week timepoint and there was no evidence suggesting soleus muscle atrophy despite continued impairment in exercise capacity at either timepoint. Therefore, we speculate that the changes at the 3-week timepoint are likely related to the hypoxia exposure rather than PH, because the animals were just removed from hypoxia exposure at the 3-week timepoint. Although there could be other mechanisms associated with the changes observed at the 3-week timepoint and we cannot completely rule out that the possibility that the recovery of fiber type at 7-week timepoint recovered any muscle dysfunction that might have happened at 3-week timepoint, the comparable exercise capacity at both 3- and 7-week timepoints suggest that the changes noted at the 3-week timepoint were not a major contributor in determining exercise capacity. In contrast to the PH SD rats, the PH CDF rats with severe PH showed soleus muscle atrophy and altered intracellular signals that occur simultaneously with RV dysfunction; however, muscle fiber types, capillary density, and the functional parameters (i.e., muscle mitochondrial function, isometric force, and fatigue profile) remain unchanged. It is also notable that despite the atrophy and molecular changes, the muscle function (ex vivo muscle contractile measurements) remains normal (Figure 7), suggesting that these changes are not sufficient to cause muscle dysfunction. Similarly, in a different skeletal muscle (i.e., EDL muscle), although there was a 10% reduction in EDL muscle mass (with no major structural changes) in the PH CDF rats, EDL muscle function remains normal reflected by unaltered mitochondrial respiration and fatigue profile (Supporting Information S1: Figure 2). These data suggest that, at least in two different skeletal muscles (soleus muscles predominantly containing Type I muscle fibers vs. EDL muscles predominantly containing Type II muscle fibers), there are same phenotypes in skeletal muscle structure and function in PH CDF rats that are not sufficient to cause exercise intolerance yet. Our results are somewhat in contrast to other studies that have

demonstrated remarkable and significant changes in fiber type distribution, atrophy, and capillary density, especially where the MCT model has been used.<sup>12,14,34–36</sup> As discussed above about the MCT-induced PH model, the discrepancy may be related to MCT-induced systemic toxicity, severe inflammation, and/or the much severe PH phenotypes with very high mortality in the MCT PH model.<sup>32,33</sup> In addition, because of the fast PH progression and very high mortality in the MCT PH rat model, these studies using MCT typically had one timepoint, by which RV dysfunction, reduced cardiac output, impaired exercise capacity, and alternations in skeletal muscles have already co-existed, which make it hard to determine causation rather than correlation.

Mitochondria are the main energy source in cells coupling the oxidation of energy substrates to the production of a high amount of ATP by the electron transport chain. Skeletal muscle mitochondrial function is recognized as a critical factor modulating exercise capacity.<sup>42</sup> In this study, we also assessed the mitochondrial respiration in skeletal muscle fibers using high-resolution O2K respirometer. Mitochondrial respiration is a key element of mitochondrial bioenergetics and reflects the function of mitochondria as structurally intact organelle.<sup>43</sup> In comparison to the static determination of molecular components in traditional methods (e.g., metabolite and enzyme levels), high-resolution O2K Respirometer offers the opportunity to dynamically measure metabolic flux and therefore provides an integrated measure of the dynamics of mitochondrial complex coupled metabolism pathways and function.<sup>43</sup> Our data showed that there were no changes in mitochondrial respiration in skeletal muscle fibers in both PH rat models, indicating that, at least in the SuHx-induced PH rat models and the timepoints we investigated, skeletal muscle mitochondrial function remains normal and does not participate in limiting exercise capacity. Interestingly, while the mitochondrial function is normal, we found some dysregulation in the signaling related to metabolism and mitochondrial regulation in soleus muscle of the PH CDF rats, including an increase in pAMPK (metabolic sensors) and PGC1 $\alpha$  (regulator of mitochondrial biogenesis) and a decrease in DRP1 and PINK1 (regulators of mitochondrial fission). This could reflect that cellular signaling changes occurring at this timepoint are not sufficient to alter the muscle function or could be an adaptive response to maintain skeletal muscle function. It is notable that our findings are consistent with the finding from patients with idiopathic pulmonary arterial hypertension showing that there is no primary mitochondrial oxidative phosphorylation dysfunction in skeletal muscle.<sup>16</sup>

Any major intrinsic change in skeletal muscles could alter muscle isometric force and fatigue profile, which are parameters directly reflecting skeletal muscle function and functional capacity in exercise. In this study, we performed *ex vivo* assessments of isometric force-frequency and fatigue profile in skeletal muscle. This approach is important, because it focuses on the skeletal muscle itself and allows direct assessment of the intrinsic properties of the skeletal muscle without impacts from the nerve and blood supply.<sup>28</sup> Consistent with our other findings described above, our data did not show any changes in muscle isometric force-frequency or fatigue profile in PH SD rats and PH CDF rats in comparison to their respective controls. These data provide strong evidence that skeletal muscle functional alterations when present occur after the appearance of reduced exercise capacity in PH.

Our study has some limitations. We investigated only soleus and EDL muscles, and we cannot exclude the possibility that other locomotor muscles may have altered muscle function in the PH rat models we used and may be able to alter exercise capacity. However, the similar phenotypes we observed in soleus and EDL muscles in the PH CDF rats suggest that this possibility is low. We assessed exercise capacity using VO<sub>2</sub> max, which is a validated and translational assessment of exercise capacity. We did not perform basal activity monitoring in this study, which could be an additional assay for physical function. We also did not assess impaired endothelial and vasomotor function in skeletal muscles (e.g., alterations in vasoconstrictive response) that can limit muscle blood perfusion during exercise.<sup>44–46</sup> While it warrants future investigation, a recent study reported that exercising skeletal muscles in PH extract oxygen to a similar level seen in healthy individuals.<sup>47</sup>

In summary, this is the first study that comprehensively evaluates intrinsic changes in soleus and EDL muscles in PH rat models. The intrinsic features that we investigated included muscle structural changes (i.e., muscle atrophy, fiber type switching, and capillary density), mitochondrial function, isometric force and fatigue profile, and alterations of signaling cascades. Importantly, this study provides direct evidence showing reduced exercise capacity in PH occurs before skeletal muscle dysfunction and suggesting that intrinsic changes in skeletal muscle are not causative to exercise intolerance in PH. Our data highlight that improving central cardiopulmonary impairments including RV function (particularly at the early stage of PH) may be critical in preventing or delaying the occurrence of exercise limitation in settings of PH. Most importantly, there remains an urgent unmet need to therapeutically

target RV dysfunction to improve PH prognosis and exercise capacity.

### AUTHOR CONTRIBUTIONS

Peng Zhang and Gaurav Choudhary gave the conception and design of the study. Peng Zhang, Denielli Da Silva Goncalves Bos, Alexander Vang, Julia Feord, Danielle J. McCullough, and Richard T. Clements performed the experiments and data acquisition. Peng Zhang, Denielli Da Silva Goncalves Bos, Richard T. Clements, and Gaurav Choudhary performed data analysis and interpretation. Peng Zhang, Denielli Da Silva Goncalves Bos, Alexandra Zimmer, and Natalie D'Silva prepared the final figures. Peng Zhang and Denielli Da Silva Goncalves Bos wrote the original draft. Peng Zhang, Denielli Da Silva Goncalves Bos, Alexander Vang, Danielle J. McCullough, Richard T. Clements, and Gaurav Choudhary reviewed and edited the manuscript. All authors reviewed and approved the final manuscript. Gaurav Choudhary is the guarantor of the content of the manuscript.

### ACKNOWLEDGMENTS

The authors are grateful to Ana Fernández Nicolás, Thomas Mancini, Amanda Costa, and Eric Wang for their technical support. The authors acknowledge assistance from core services supported by the National Institute of General Medical Science of the National Institutes of Health under grant number P20GM103652. This study was supported by VA Merit Review I01CX001892 (G. C.) and NHLBI R01HL148727 (G. C.). P. Z. was also supported by NIGMS/NIH 5P20GM103652. R. T. C. was supported by NHLBI R01HL135236. The views expressed in this article are those of the authors and do not reflect the position nor policy of the Department of Veterans Affairs and the National Institutes of Health.

### CONFLICT OF INTEREST STATEMENT

The authors declare no conflict of interest.

### ETHICS STATEMENT

All animal work was approved by the Institutional Animal Care and Use Committee at the Providence VA Medical Center (Approval Numbers: IACUC-2019-009 and IACUC-2020-003) and conformed with the Health Research Extension Act, US Public Health Service, and US National Institutes of Health policy.

### ORCID

Gaurav Choudhary  <http://orcid.org/0000-0001-9343-5481>

### REFERENCES

- Humbert M, Kovacs G, Hoepfer MM, Badagliacca R, Berger RMF, Brida M, Carlsen J, Coats AJS, Escribano-Subias P, Ferrari P, Ferreira DS, Ghofrani HA, Giannakoulas G, Kiely DG, Mayer E, Meszaros G, Nagavci B, Olsson KM, Pepke-Zaba J, Quint JK, Rådegran G, Simonneau G, Sitbon O, Tonia T, Toshner M, Vachiery JL, Vonk Noordegraaf A, Delcroix M, Rosenkranz S. 2022 ESC/ERS guidelines for the diagnosis and treatment of pulmonary hypertension. *Eur Respir J*. 2023;61:2200879.
- M.M. Vanhoof J, Delcroix M, Vandeveld E, Denhaerynck K, Wuyts W, Belge C, Dobbels F. Emotional symptoms and quality of life in patients with pulmonary arterial hypertension. *J Heart Lung Transplant*. 2014;33:800–8.
- Babu AS, Arena R, Morris NR. Evidence on exercise training in pulmonary hypertension. *Adv Exp Med Biol*. 2017;1000:153–72.
- Fowler RM, Gain KR, Gabbay E. Exercise intolerance in pulmonary arterial hypertension. *Pulm Med*. 2012;2012:1–10.
- Tran DL, Lau EMT, Celermajer DS, Davis GM, Cordina R. Pathophysiology of exercise intolerance in pulmonary arterial hypertension. *Respirology*. 2018;23:148–59.
- Malenfant S, Lebreton M, Breton-Gagnon É, Potus F, Paulin R, Bonnet S, Provencher S. Exercise intolerance in pulmonary arterial hypertension: insight into central and peripheral pathophysiological mechanisms. *Eur Respir Rev*. 2021;30:200284.
- Ryan JJ, Archer SL. The right ventricle in pulmonary arterial hypertension: disorders of metabolism, angiogenesis and adrenergic signaling in right ventricular failure. *Circ Res*. 2014;115:176–88.
- Tello K, Seeger W, Naeije R, Vanderpool R, Ghofrani HA, Richter M, Tedford RJ, Bogaard HJ. Right heart failure in pulmonary hypertension: diagnosis and new perspectives on vascular and direct right ventricular treatment. *Br J Pharmacol*. 2021;178:90–107.
- Manders E, Ruiter G, Bogaard HJ, Stienen GJM, Vonk-Noordegraaf A, de Man FS, Ottenheijm CAC. Quadriceps muscle fibre dysfunction in patients with pulmonary arterial hypertension. *Eur Respir J*. 2015;45:1737–40.
- Riou M, Pizzimenti M, Enache I, Charloix A, Canuet M, Andres E, Talha S, Meyer A, Geny B. Skeletal and respiratory muscle dysfunctions in pulmonary arterial hypertension. *J Clin Med*. 2020;9:410.
- Meyer FJ. Respiratory muscle dysfunction in idiopathic pulmonary arterial hypertension. *Eur Respir J*. 2005;25:125–30.
- Wüst RCI, Myers DS, Stones R, Benoist D, Robinson PA, Boyle JP, Peers C, White E, Rossiter HB. Regional skeletal muscle remodeling and mitochondrial dysfunction in right ventricular heart failure. *Am J Physiol Heart Circ Physiol*. 2012;302:H402–11.
- Breda AP, Pereira de Albuquerque AL, Jardim C, Morinaga LK, Suesada MM, Fernandes CJC, Dias B, Lourenço RB, Salge JM, Souza R. Skeletal muscle abnormalities in pulmonary arterial hypertension. *PLoS One*. 2014;9:e114101.
- Enache I, Charles AL, Bouitbir J, Favret F, Zoll J, Metzger D, Oswald-Mammosser M, Geny B, Charloix A. Skeletal muscle

- mitochondrial dysfunction precedes right ventricular impairment in experimental pulmonary hypertension. *Mol Cell Biochem.* 2013;373:161–70.
15. Malenfant S, Potus F, Mainguy V, Leblanc E, Malenfant M, Ribeiro F, Saey D, Maltais F, Bonnet S, Provencher S. Impaired skeletal muscle oxygenation and exercise tolerance in pulmonary hypertension. *Med Sci Sports Exerc.* 2015;47:2273–82.
  16. Sithamparamanathan S, Rocha MC, Parikh JD, Rygiel KA, Falkous G, Grady JP, Hollingsworth KG, Trenell MI, Taylor RW, Turnbull DM, Gorman GS, Corris PA. Skeletal muscle mitochondrial oxidative phosphorylation function in idiopathic pulmonary arterial hypertension: in vivo and in vitro study. *Pulm Circ.* 2018;8:1–5.
  17. Larson L, Lioy J, Johnson J, Medler S. Transitional hybrid skeletal muscle fibers in rat soleus development. *J Histochem Cytochem.* 2019;67:891–900.
  18. Clements RT, Vang A, Fernandez-Nicolas A, Kue NR, Mancini TJ, Morrison AR, Mallem K, McCullough DJ, Choudhary G. Treatment of pulmonary hypertension with angiotensin II receptor blocker and neprilysin inhibitor sacubitril/valsartan. *Circ Heart Fail.* 2019;12:e005819.
  19. Mendiola EA, da Silva Goncalves Bos D, Leichter DM, Vang A, Zhang P, Leary OP, Gilbert RJ, Avazmohammadi R, Choudhary G. Right ventricular architectural remodeling and functional adaptation in pulmonary hypertension. *Circ Heart Fail.* 2023;16:e009768.
  20. Vang A, da Silva Gonçalves Bos D, Fernandez-Nicolas A, Zhang P, Morrison AR, Mancini TJ, Clements RT, Polina I, Cypress MW, Jhun BS, Hawrot E, Mende U, O-Uchi J, Choudhary G.  $\alpha 7$  nicotinic acetylcholine receptor mediates right ventricular fibrosis and diastolic dysfunction in pulmonary hypertension. *JCI Insight.* 2021;6:e142945.
  21. McCullough DJ, Kue N, Mancini T, Vang A, Clements RT, Choudhary G. Endurance exercise training in pulmonary hypertension increases skeletal muscle electron transport chain supercomplex assembly. *Pulm Circ.* 2020;10:1–11.
  22. González-Saiz L, Fiuza-Luces C, Sanchis-Gomar F, Santos-Lozano A, Quezada-Loaiza CA, Flox-Camacho A, Munguía-Izquierdo D, Ara I, Santalla A, Morán M, Sanz-Ayan P, Escribano-Subías P, Lucia A. Benefits of skeletal-muscle exercise training in pulmonary arterial hypertension: the WHOLEi+12 trial. *Int J Cardiol.* 2017;231:277–83.
  23. Wisløff U, Helgerud J, Kemi OJ, Ellingsen Ø. Intensity-controlled treadmill running in rats: VO<sub>2</sub> max and cardiac hypertrophy. *Am J Physiol Heart Circ Physiol.* 2001;280:H1301–10.
  24. Baldwin KM, Cooke DA, Cheadle WG. Time course adaptations in cardiac and skeletal muscle to different running programs. *J Appl Physiol.* 1977;42:267–72.
  25. Dudley GA, Abraham WM, Terjung RL. Influence of exercise intensity and duration on biochemical adaptations in skeletal muscle. *J Appl Physiol.* 1982;53:844–50.
  26. Bedford TG, Tipton CM, Wilson NC, Oppliger RA, Gisolfi CV. Maximum oxygen consumption of rats and its changes with various experimental procedures. *J Appl Physiol.* 1979;47:1278–83.
  27. de Man FS, van Hees HWH, Handoko ML, Niessen HW, Schalij I, Humbert M, Dorfmueller P, Mercier O, Bogaard HJ, Postmus PE, Westerhof N, Stienen GJM, van der Laarse WJ, Vonk-Noordegraaf A, Ottenheim CAC. Diaphragm muscle fiber weakness in pulmonary hypertension. *Am J Respir Crit Care Med.* 2011;183:1411–8.
  28. Park KH, Brotto L, Lehoang O, Brotto M, Ma J, Zhao X. Ex vivo assessment of contractility, fatigability and alternans in isolated skeletal muscles. *J Vis Exp.* 2012;69:e4198.
  29. Pesta D, Gnaiger E. High-resolution respirometry: OXPHOS protocols for human cells and permeabilized fibers from small biopsies of human muscle. *Methods Mol Biol.* 2012;810:25–58.
  30. Suen CM, Chaudhary KR, Deng Y, Jiang B, Stewart DJ. Fischer rats exhibit maladaptive structural and molecular right ventricular remodeling in severe pulmonary hypertension: a genetically prone model for right heart failure. *Cardiovasc Res.* 2019;115:788–99.
  31. Myers J, Prakash M, Froelicher V, Do D, Partington S, Atwood JE. Exercise capacity and mortality among men referred for exercise testing. *N Engl J Med.* 2002;346:793–801.
  32. Colvin KL, Yeager ME. Animal models of pulmonary hypertension: matching disease mechanisms to etiology of the human disease. *J Pulm Respir Med.* 2014;4:198.
  33. Gomez-Arroyo JG, Farkas L, Alhussaini AA, Farkas D, Kraskauskas D, Voelkel NF, Bogaard HJ. The monocrotaline model of pulmonary hypertension in perspective. *Am J Physiol Lung Cell Mol Physiol.* 2012;302:L363–9.
  34. Moreira-Gonçalves D, Padrão AI, Ferreira R, Justino J, Nogueira-Ferreira R, Neuparth MJ, Vitorino R, Fonseca H, Silva AF, Duarte JA, Leite-Moreira A, Henriques-Coelho T. Signaling pathways underlying skeletal muscle wasting in experimental pulmonary arterial hypertension. *Biochim Biophys Acta.* 2015;1852:2722–31.
  35. Vescovo G. Skeletal muscle myosin heavy chain expression in rats with monocrotaline-induced cardiac hypertrophy and failure. Relation to blood flow and degree of muscle atrophy. *Cardiovasc Res.* 1998;39:233–41.
  36. dalla Libera L, Zennaro R, Sandri M, Ambrosio GB, Vescovo G. Apoptosis and atrophy in rat slow skeletal muscles in chronic heart failure. *Am J Physiol Cell Physiol.* 1999;277:C982–6.
  37. Jiang B, Deng Y, Suen C, Taha M, Chaudhary KR, Courtman DW, Stewart DJ. Marked strain-specific differences in the SU5416 rat model of severe pulmonary arterial hypertension. *Am J Respir Cell Mol Biol.* 2016;54:461–8.
  38. Savarese G, Musella F, D'Amore C, Losco T, Marciano C, Gargiulo P, Rengo G, DelleGrottaglie S, Bossone E, Leosco D, Perrone-Filardi P. Haemodynamics, exercise capacity and clinical events in pulmonary arterial hypertension. *Eur Respir J.* 2013;42:414–24.
  39. Mainguy V, Maltais F, Saey D, Gagnon P, Martel S, Simon M, Provencher S. Peripheral muscle dysfunction in idiopathic pulmonary arterial hypertension. *Thorax.* 2010;65:113–7.
  40. Batt J, Ahmed SS, Correa J, Bain A, Granton J. Skeletal muscle dysfunction in idiopathic pulmonary arterial hypertension. *Am J Respir Cell Mol Biol.* 2014;50:74–86.
  41. Potus F, Malenfant S, Graydon C, Mainguy V, Tremblay È, Breuils-Bonnet S, Ribeiro F, Porlier A, Maltais F, Bonnet S, Provencher S. Impaired angiogenesis and peripheral muscle microcirculation loss contribute to exercise intolerance in

- pulmonary arterial hypertension. *Am J Respir Crit Care Med.* 2014;190:318–28.
42. Zoll J, Sanchez H, N'Guessan B, Ribera F, Lampert E, Bigard X, Serrurier B, Fortin D, Geny B, Veksler V, Ventura-Clapier R, Mettauer B. Physical activity changes the regulation of mitochondrial respiration in human skeletal muscle. *J Physiol.* 2002;543:191–200.
  43. Doerrier C, Garcia-Souza LF, Krumschnabel G, Wohlfarter Y, Mészáros AT, Gnaiger E. High-resolution FluoRespirometry and OXPHOS protocols for human cells, permeabilized fibers from small biopsies of muscle, and isolated mitochondria. *Methods Mol Biol.* 2018;1782:31–70.
  44. Budhiraja R, Tuder RM, Hassoun PM. Endothelial dysfunction in pulmonary hypertension. *Circulation.* 2004;109:159–65.
  45. Stewart DJ, Levy RD, Cernacek P, Langleben D. Increased plasma endothelin-1 in pulmonary hypertension: marker or mediator of disease? *Ann Intern Med.* 1991;114:464–9.
  46. Wray DW, Nishiyama SK, Donato AJ, Sander M, Wagner PD, Richardson RS. Endothelin-1-mediated vasoconstriction at rest and during dynamic exercise in healthy humans. *Am J Physiol Heart Circ Physiol.* 2007;293:H2550–6.
  47. Stubbs H, Church C, Johnson M, Thomson S. Impairment of skeletal muscle oxygen extraction and cardiac output are matched in precapillary pulmonary hypertension. *ERJ Open Res.* 2021;7:00449-2021.

## SUPPORTING INFORMATION

Additional supporting information can be found online in the Supporting Information section at the end of this article.

**How to cite this article:** Zhang P, Da Silva Goncalves Bos D, Vang A, Feord J, McCullough DJ, Zimmer A, D'Silva N, Clements RT, Choudhary G. Reduced exercise capacity occurs before intrinsic skeletal muscle dysfunction in experimental rat models of pulmonary hypertension. *Pulm Circ.* 2024;14:e12358. <https://doi.org/10.1002/pul2.12358>